Journal of Motor Behavior, 1993, Vol. 25, No. 3, 175-192

Models of Trajectory Formation and Temporal Interaction of Reach and Grasp

Bruce Hoff
Hughes Research Laboratories
Malibu, California

Michael A. Arbib
Center for Neural Engineering
University of Southern California

ABSTRACT. Our goal was to create a principled account of a body of behavioral kinematic data on reaching and grasping. We show how to transform an optimality principle for overall hand transport into a feedback control law and then incorporate look-ahead modules in the controller to compensate for delays in sensory feedback. This model describes the kinematics of hand transport under a variety of circumstances, including target perturbations. We then develop a model for the temporal coordination of reach and grasp. We provide an optimization principle for hand preshaping that trades off the costs of maintaining the hand in an open position and the cost of accelerating the change in grip size. This yields a control system for preshaping. We then show that a model that uses only expected duration for coordination, rather than kinematic or dynamic variables, can describe the kinematics of interaction of hand transport and preshape under a variety of circumstances, including perturbations of object position and object size.

Key words: coordination, grasp, model, optimization, reach

1. Introduction

Our original interest in hand transport and preshaping arose from the work of Jeannerod (1981; see also Jeannerod & Biguer, 1982), who studied the shaping of the hand as it moved from its initial position to pick up a ball. The hand was *preshaped* so that when it had almost reached the ball, it was of the right shape and orientation to enclose the ball prior to gripping it firmly. By examining consecutive frames of a movie, one could see that the movement was divided into two parts, a fast initial movement and a slow approach movement. This led to the coordinated control program for the behavior shown in Figure 1a (Arbib, 1981). In the top half of the figure, we see three perceptual schemas—schemas whose job it is to find information about the environment rather than to control movement. Solid lines indicate the transfer of data from one schema to another, and dashed lines indicate the transfer of activation. Successful completion of the task of locating the object activates schemas for recognizing the size and orientation of the object. The outputs of these perceptual schemas are available on separate channels for the control of the hand movement. This in turn involves the concurrent activation of two motor schemas, or control systems. One moves the arm to transport the hand toward the object, the other preshapes the hand, with the fingers' separation and orientation guided by the output of the appropriate perceptual schemas. Note that, in this model, once the hand is preshaped, the schema involved in shaping the hand "goes to sleep." It is only the completion of the fast phase of hand transfer that triggers the slow phase of hand transfer as well as "wakes up" the final stage of the grasping schema, which, under control of tactile feedback, will shape the fingers.

Subsequent experimental findings have shown that the model of Figure 1a was no longer tenable. Wing, Turton, and Fraser (1986) found that peak grip aperture increased with variability of reach, caused either by reaching more quickly or reaching with the eyes closed. Recent experiments from Jeannerod's laboratory, to be discussed further, showed that during perturbation of either target location or size, both arm reaching and preshaping of the fingers were affected. Observations such as these showed that there is more interaction between the two motor processes than previously thought. Further, whereas the model of Figure 1a provides a preliminary explanation of transport/preshape interaction, it does not address the trajectory formation, which, as we will see, reflects subtle effects of the interaction of the two motor processes. The task of the present article is to provide an updated model that addresses new data on how hand trajectories vary in visually guided reaching tasks when the target is perturbed during the movement. The two major changes to the model are as follows: (a) The transport schema cannot be divided into two separate phases, the first of which is ballistic, but must instead be

Correspondence address: Bruce Hoff, Hughes Research Laboratories, 3011 Malibu Canyon Road, Malibu, CA 90265.

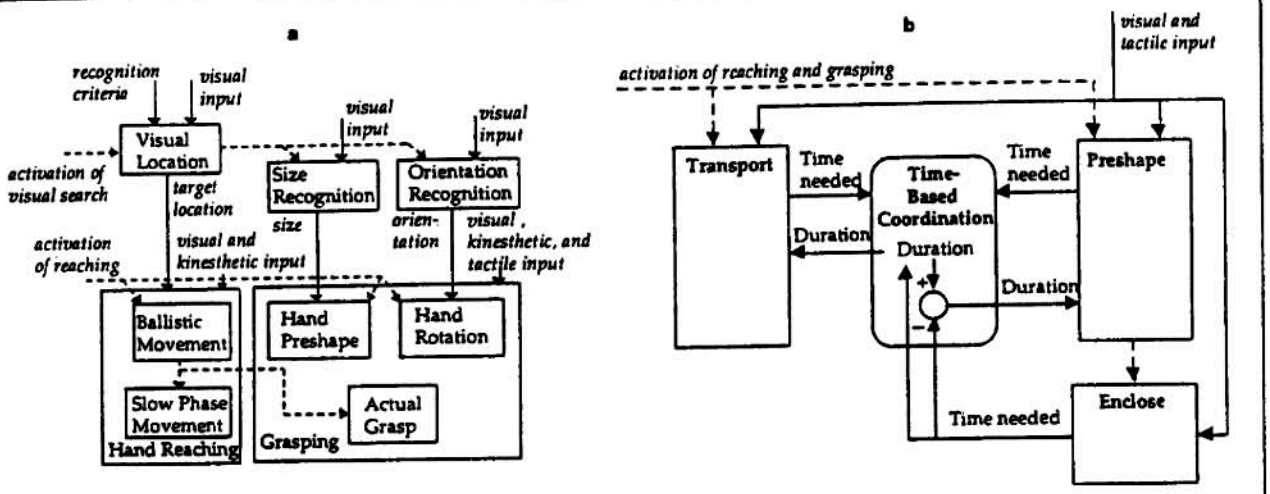

FIGURE 1. (a) Coordinated control program for reach and grasp. (b) An overview of the new model of the motor schemas, and their coordination through timing, that is presented in this article. (Redrawn from Figure 14, p. 1468 of "Perceptual Structures and Distributed Motor Control," by M. A. Arbib, 1981.) In V. B. Brooks (Ed.). *Handbook of Physiology: Sec. 1. The nervous system: Vol. 2. Motor Control* (pp. 1449-1480). Copyright 1981 by The American Physiological Society. Reprinted by permission.

modeled as a single feedback system. The latencies within that system make fast movements appear to be ballistic in all but their final portions. (b) The one-way flow of activation from the transport to the grasp schema must be replaced by a two-way interaction. We postulate that this interaction is mediated solely by timing relations. A high-level overview of the new motor schemas is presented in Figure 1b. The details of their operation and interaction are provided in the remainder of this article.

In Section 2, we consider only the transport of the hand; in Section 3 we address the coordinated hand and finger movements involved in grasping. To model hand transport, we combined the minimum-jerk optimality principle for overall hand transport with a feedback control law and then incorporated look-ahead modules in the controller to compensate for delays in sensory feedback to show how the central nervous system (CNS) may form a desired kinematic reaching trajectory while using delayed feedback of both hand and target position to ensure that the hand approaches its target despite mechanical noise or perturbation of the target (Hoff & Arbib, 1991). The model reproduces observed properties of reaching in response to target perturbation, and results of computer simulation of this model are presented.

In Section 3, we extend the model of reaching to explain both the kinematics of hand preshape for prehension and the temporal interactions of reach and grasp. We provide an optimization principle for hand preshaping that trades off the costs of maintaining the hand in an open position and the cost of accelerating the change in grip size. This yields a control system for preshaping. We then present a model that uses only expected duration for coordination of transport and preshape. We show through computer simulation that the model can describe the kinematics of interaction of hand transport and preshape under a variety of circumstances, including perturbations of object position and object size.

2. Modeling Perturbation Response in Reaching

This section briefly reviews the model presented by Hoff and Arbib (1991) as background for the novel model offered in Section 3.

2.1 Background

Hogan (1984) proposed the *minimum-jerk* hypothesis to describe the kinematics in pointing movements of monkeys toward a visually located target. This is the hypothesis that a trajectory of duration t_f will be such as to minimize the integral $\int_0^{t_f} (d^3x/dt^3)^2 dt$ of the square of the *jerk*, which is the derivative of acceleration. By applying the calculus of variations, he derived a position function of time given by a fifth-order polynomial, uniquely specified by the initial and final values of position, velocity, and acceleration. If the target has zero velocity and acceleration at the start and end of the movement, the velocity profile is symmetric and bell-shaped, much like the low-accuracy pointing movements performed by the subjects. Related studies (Atkeson & Hollerbach, 1985; Flash, 1987; Flash & Hogan, 1985) provided strong evidence that a single kinematic pattern for voluntary limb movements exists for a variety of conditions.

Evidence that the characteristic movement profiles are developed as the movement unfolds and subject to modification by sensory input during the reaching movement came from target perturbation experiments that showed that reaching movements can be modified "on the fly." This

implies a system that reevaluates its progress as movement proceeds, based on incoming, albeit delayed, sensory information. Pélisson, Preblanc, Goodale, and Jeannerod (1986) perturbed the target of a pointing task at movement onset. The initial target was 30, 40, or 50 cm from the hand's starting position, and the perturbed target position was 10% farther away. Vision of the subjects' hand was prevented, and they consistently undershot the target. When the target was perturbed, however, the distance moved increased an amount corresponding to the perturbation. Also, the subject did not stop before moving on to the new target. Rather, a smooth transition was made (without secondary accelerations) in midflight to a new trajectory terminating farther away (Figure 3a). The subject was often unaware that the target had moved. Because the corrections were performed without vision of the arm, these results also imply that we use kinesthetic information and/or an internal model of the arm to update the motor error and the reaching program in real time. Georgopoulos, Kalaska, and Massey (1981) found a prompt transition to a new trajectory after target perturbation when they observed monkeys trained to make planar arm movements. The monkeys made reaching movements to single targets and to targets that switched either to a nearby location or to one on the opposite side of the starting point. The time of target perturbation was varied from 50 to 400 ms after the first target was presented. They found a reaction time of 260 ms both for the initiation of movement to the first target and for the modification of the trajectory to reach a suddenly appearing new target. Thus, as in the observations of Pélisson et al. (1986), primary movement completion was not necessary before implementing a novel trajectory.

Paulignan, MacKenzie, Marteniuk, and Jeannerod (1991) perturbed the location of a vertically oriented dowel upon initiation of a reaching movement toward the dowel. Recording the kinematics of reaching and grasping under normal and perturbed conditions, they noted trajectory adjustment within 100 ms (on the average) after target location perturbation, without compromise of accuracy (that is, there were no trials in which the subject failed to grasp the dowel). The movements, which when unperturbed lasted about 500 ms, lasted about 100 ms longer when the target was shifted at movement onset, indicating on-line incorporation of novel sensory information. Another interesting aspect of this study was of variability during movement. They found that the standard deviation of position in the path reached a maximum of about 25 mm during the movement, whereas the standard deviation of the final position was about 5 mm. This implies that, although motor variability caused significant deviation in the path during the movement, some feedback mechanism stabilized the trajectory toward the end. The feedback aspect of trajectory generation was not taken into account in feedforward models such as that of Schmidt, Zelaznik, and Frank (1977). Further, as emphasized by Meyer, Abrams, Kornblum, Wright, and Smith (1988), models of trajectory formation that do not have variability as an element, such as the iterative correction model (Craik, 1947), are not realistic. In the model that we developed here, noise was added throughout the movement. This resulted in the more realistic model in which each point in the movement has its individual variability. The overall cumulative movement variability is then compensated by a feedback mechanism, to a degree determined by the duration of the movement.

2.2 A New Model of Perturbation Response in Reach

We now turn to the model of hand transport offered by Hoff and Arbib (1991).[1] We saw in our discussion of Figure 1a that the reach-to-grasp movement has been characterized as a two-phase process, with a quick forward phase followed by a slow feedback phase (Jeannerod, 1984; Woodworth, 1899). Here, in view of the above data on variability and on target perturbation, we argue that for free space pointing and reaching to grasp, a single feedback process can be responsible both for the quick phase and for the slow, accurate phase.[2] This uniform feedback process may be kinesthetically based, as well as visually based, providing shorter feedback latency. The output of our system for trajectory generation is based both on internal dynamics and on feedback from the outside, and includes a stochastic element to model variability and demonstrate robustness.

The minimum-jerk criterion predicts, for any stationary start and end points, a straight-line path for the hand, whose displacement along the straight path is given by a quintic polynomial in time (Flash & Hogan, 1985). The coefficients of this polynomial are determined by the boundary conditions—the starting and ending position, velocity, and acceleration of the hand. We thus view the system state as $q = (x, v, a)^T$ (the ordered triple of position, velocity, and acceleration; where T denotes the transpose). Flash and Hogan (1985) derived the coefficients of the quintic for the hand's position when the initial and final states are at rest, and showed that the resulting trajectories accurately model planar, point-to-point arm movements. The implication is that trajectory planning and optimization maybe done in *end-point* space, with lower-level computations' producing the appropriate muscle activations. The model developed below is one of continuous control based on this minimum-jerk principle, extending the set of results to include target perturbation response and motor variability. The movement boundary conditions may be generalized to allow a non-static initial state $(x_0, v_0, a_0)^T$, but a static final state $(x_f, 0, 0)^T$ with target position x_f (Flash & Hogan, 1985; Hoff & Arbib, 1991). In considering the hand's acceleration (second derivative of position and hence a cubic polynomial), these boundary conditions yielded the following expression:

$$\begin{aligned} a(t) = {} & a_0[1 - 9\tau + 18\tau^2 - 10\tau^3] \\ & + v_0[-36\tau + 96\tau^2 - 60\tau^3]/D \\ & + (x_f - x_0)[60\tau - 180\tau^2 + 120\tau^3]/D^2, \end{aligned} \tag{1}$$

where the movement begins at $t = t_0$ and ends at $t = t_f$, so that $D = t_f - t_0$ is the duration and $\tau = (t - t_0)/D$ is the

normalized time variable. Then, to allow for perturbations in the arm's state or the target location, we considered a feedback controller that inherently compensates for perturbations during motion. The form of such a system is

$$q' = Aq + Bx_t, \tag{2}$$

where $q = (x, v, a)^T$ is the system state vector, and the matrix A and vector B embody the system dynamics. From (1), Hoff and Arbib (1991) readily showed that A and B take the form

$$A = \begin{bmatrix} 0 & 1 & 0 \\ 0 & 0 & 1 \\ -60/D^3 & -36/D^2 & -9/D \end{bmatrix}, \quad B = \begin{bmatrix} 0 \\ 0 \\ 60/D^3 \end{bmatrix}, \tag{3}$$

where again D is the time remaining in the movement, $D = t_f - t$. In this formulation, the controller need not store an entire temporal trajectory. It need generate only D, the time remaining, and monitor the current state q and target x_t. This is an important difference from the feedforward formulation; for here, if at any instant the state is perturbed from q to another state $\tilde{q}$ at time $\tilde{t}$, the system then proceeds along the (new) optimal trajectory from $\tilde{q}$ to the target state $(x_t, 0, 0)^T$ in time $D = t_f - \tilde{t}$. Further, if the target moves so that there is a new final state, $(\hat{x}_t, 0, 0)^T$, then the system proceeds along the optimal trajectory to this new target. The impact of this model on simulation of reaching to perturbed targets is shown below.

Because of the linear system formulation of Equation 2, the resulting kinematic trajectory $q(t)$ scales with the input, that is, the target distance $x_t - x_o$. Thus, the model duplicates the findings of MacKenzie, Marteniuk, Dugas, Liske, and Eickmeier (1987) that peak velocity (along with the rest of the kinematic profile) scales with movement amplitude.

The implementation of this feedback trajectory-generator mechanism is shown in Figure 2a. We assumed that the trajectory for the hand is specified in terms of its acceleration kinematics, shown as the input a to the box labeled *inverse dynamics and plant*. This label emphasizes that this is a kinematics model, not accounting for the forces, muscle activations, and limb dynamics involved in moving the arm. We assumed that within this box the desired kinematic trajectory (expressed in terms of time varying acceleration) is translated into the appropriate driving forces to move the arm. The output of this box is then the resulting position (x) and velocity (v) of the hand. (Although the inverse dynamics subproblem is not addressed here, modeling efforts such as those of Kawato, Miyamoto, Setoyama, & Suzuki, 1988, have studied it at length.) The box labeled *feedback unit* performs the computation obtained by taking the derivative of Equation 1 with respect to $t = \tau D$ and setting τ to 0; namely,

$$f = -9a/D - 36v/D^2 + 60(x_t - x)/D^3, \tag{4}$$

after which f is integrated to yield the driving acceleration signal.

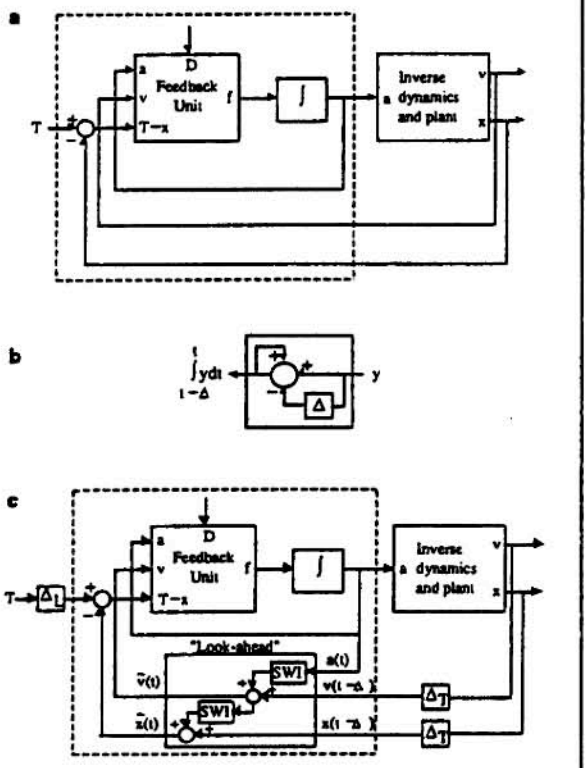

FIGURE 2. Using feedback to generate a time-varying trajectory. (a) A mechanism for generating a state trajectory by mapping the current state and target into a control signal. (b) The computational module for a sliding window integrator (SWI), integrating the input (u) over time for the past (Δ) time interval. It is used in (c) (box labeled *SWI*) as part of the state look-ahead module. (c) Extension of (a) to accept delayed feedback by calculating the estimates of the present state, based on the efferent command to the plant and delayed feedback, to compensate for noise.

The problem that we must now address is that Figure 2a uses instantaneous feedback, whereas, in reality, the current target position and hand v and x are sensed with some latency. Hoff and Arbib (1991) solved this by means of a *look-ahead unit*, a sliding window integrator (SWI) whose output is the integral of its input over the most recent time period Δ, $z = \int_{t-\Delta}^{t} v dt$.[3] This construction is shown in Figure 2b, where the box labeled Δ indicates a temporal delay and the positive feedback line indicates the integration. It is used in Figure 2c (the boxes labeled *SWI*) to estimate the plant's position and velocity from delayed feedback in the presence of noise. If the noise is unbiased, this is the most reasonable estimate of the current state.

The delayed feedback model is pictured in Figure 2c. Position and velocity feedback are both delayed by an amount Δ_T. (Note that this delay represents the collective delay for the sensorimotor loop, both the time for external events to affect the internal program, i.e., sensory delay,

and the time for the internal program to influence movement kinematics, i.e., motor delay.) To compensate for this delay, we included a *state look-ahead* module to estimate the current plant state. Essentially, because it computes only movement kinematics, it performs a double integral of the control signal, $a(t)$, to estimate the change in $x(t)$ during the delay period (and also the change in $v[t]$, along the way) and uses these values to extrapolate from the delayed state values to an estimate of the present value. With no mechanical noise or unexpected perturbations of the hand, the look-ahead module gives a precise prediction. (Note also that the perception of target position encounters delay. To indicate that this delay need not be the same length as the arm state delay, we labeled it Δ_L.) The present position estimate, generated by the look-ahead module, is subtracted from this delayed target location to yield motor error. The effect of this target location delay is significant in the perturbed target paradigm, where the kinematic responses to a shifting target is delayed by an amount Δ_L.

Having presented this feedback control model of reach generation, which operates in the presence of noise and delayed information, in the next section we present the results of simulations of this model to explain behavioral data on response to target perturbation.

2.3 Simulation Results

We simulated the reach generator of Figure 2 both for noisy and for perturbed target situations, modeling a one-dimensional (1-D) movement trajectory. The controllable parameters of the simulation were movement amplitude (x_t), movement duration (MT), noise amplitude (NA), the displacement (δx_t) and time of onset of target perturbation, and the increase in movement time after target perturbation. Noise in the system was simulated as a random value, uniformly distributed in an interval $(-R/2, +R/2)$ superimposed on the movement velocity, where $R = NA \times V$, the controllable parameter NA (set to 0.10 times the current velocity) in the simulations to be discussed. The simulation output consisted of position, velocity, and acceleration profiles, which we collected for each simulated reach. To simulate target movement, we shifted the target in one step from x_t to $x_t + \delta x_t$, and extended movement duration from MT to $MT + \delta MT$, so that the value of D in Equation 4, after the shift, was increased by δMT.

Addressing the target perturbation experiment of Pélisson et al. (1986) discussed earlier, we simulated the effect of perturbing target position at movement onset, assuming a feedback delay of 100 ms and a movement amplitude that increased from 40 cm to 44 cm. Allotted movement time was initially 520 ms and increased to 540 ms after perturbation, both time values within the range of measured movement times for the corresponding distance. The result is seen in Figures 3b and c. At the qualitative level, there were the generally bell-shaped velocity profile and the double-peaked acceleration profile in both the model and in the data. Further, the transition to the new trajectory in Figure 3c was seamless, as seen in the actual data of Figure 3a. Our model of continuous comparison between target position and arm state correctly predicted the smooth transition. (This result was in contrast to the characteristic transitions during backward and sideways target perturbations, seen in the data and reproduced by the model, below and in Section 3.) Quantitatively, in both the data and modeling results, peak velocity occurred halfway through the movement (at 260 ms) in the unperturbed case, with a slight increase in its time of occurrence in the perturbed case (at 270 ms in the data, 280 ms in the model). The magnitudes of peak velocity and acceleration were affected very little by perturbation, as seen both in the model and data. These values were only slightly lower in the model than in the data. Peak velocity was 220 cm/s in the data, 144 cm/s in the model. Peak acceleration was about 1,000 cm/s^2 in the data, 850 cm/s^2 in the model. The important result to emphasize was the lack of interruption of the trajectory after perturbation of the target location.

A trajectory transition was observable when the target of reach was perturbed significantly in location and direction from the hand's starting position, as in the trajectory reversal experiment of Georgopoulos et al. (1981). To see whether our model duplicated their subject's movement profile, we used the distance and timing parameters from their data to run the target perturbation simulation. We simulated the movement, shown in Figure 4, of reaching to a target 8 cm away from the hand's initial position, which then switched to a point 8 cm behind the initial position, 50 ms before the onset of the initial movement. The trajectory perturbation began 200 ms into the simulated movement because of sensory delay. In the simulation, the chosen movement time parameter directly affected peak velocity: Longer movement time meant lower peak velocity. Using an initial movement time of 260 ms (taken from their data for the unperturbed case) and a modified movement time of 350 ms taken from the perturbed case (Figure 4a), we found, as did they, a higher secondary velocity peak than the first. The ratio of the second peak height to the first in their data was 1.62, and in our simulation (Figure 4b), 1.69. The timing of the occurrence of the peaks was also the same: The first peak occurred 130 ms after movement onset in the data, at 120 ms in the model. The second velocity peak occurred at 340 ms in the data, 350 ms in the model. The time of movement reversal was 210 ms in the data, 230 ms in the model. Thus the kinematics of target reversal in the simulation were similar to those seen in the behaving subject: The response to perturbation was delayed only by the nominal reaction time; and to reverse the trajectory, a significantly higher velocity curve was created, whose kinematic landmarks (peak velocity and time of reversal) occurred at realistic times.

We have described a limb movement-generation model that admits target perturbations during movement. Its output is in terms of hand kinematics, and so is comparable with data from experiments on human's and monkey's motor behavior. The model explicitly shows how a family of movement trajectories might be generated by a controller

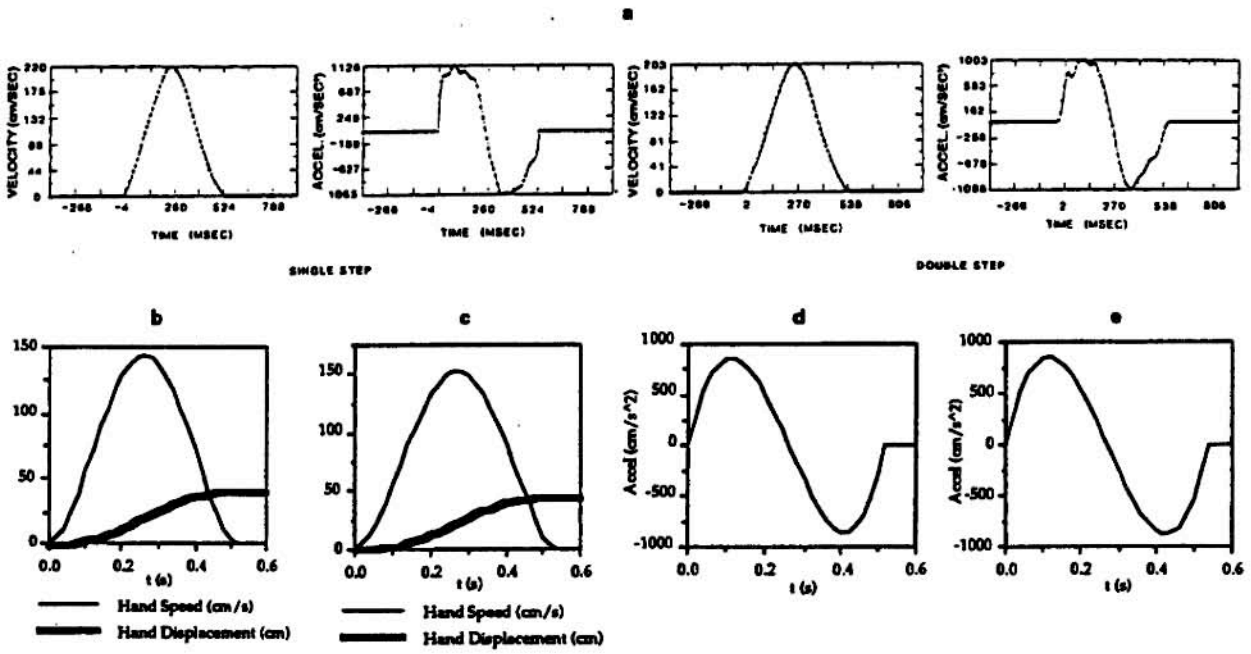

FIGURE 3. Target perturbation experiment of Pélisson et al. (1986). (a) Hand velocity and acceleration profiles for unperturbed reach to 40-cm target (left) and perturbed reach, from 40 to 44 cm (right). (b) Simulation of unperturbed reach, showing position and velocity profiles. (c) Simulation of target perturbation response, showing a seamless transition to a corrective trajectory in response to a small target perturbation. Also shown is acceleration for (d) unperturbed and (e) perturbed cases. *Note.* The data in part a are from "Visual Control of Reaching Movements Without Vision of the Limb: II. Evidence of Fast, Unconscious Processes Correcting the Trajectory of the Hand to the Final Position of a Double-Step Stimulus" by D. Pélisson, C. Prablanc, M. A. Goodale, and M. Jeannerod, 1986, *Experimental Brain Research, 62,* 303-311. Copyright 1986 by Springer-Verlag Publishers. Reprinted by permission.

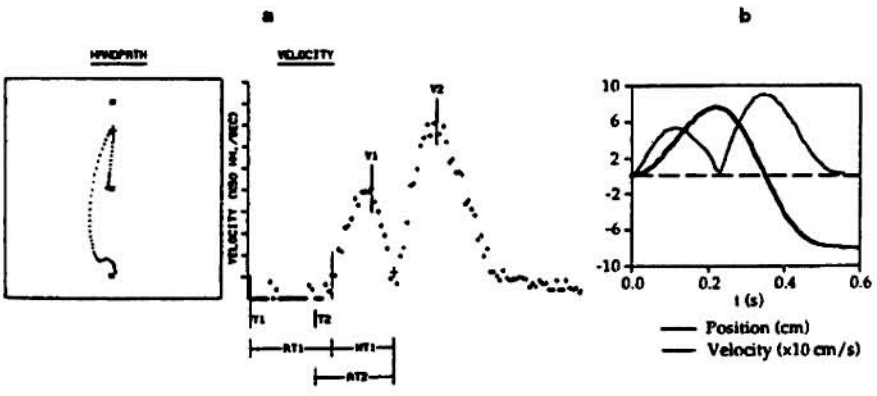

FIGURE 4. Direction reversal experiment of Georgopoulos, Kalaska, and Massey (1981). (a) Actual data. Left, top view of hand path; right, speed profile, points spaced by 10 ms. (b) Simulation. A monkey moves a planar manipulandum to capture indicated targets, which are 8 cm from the starting position, in opposite directions. Position and absolute value of velocity (× 10 cm/s) are shown. *Note.* The data in part a are from "Spatial Trajectories and Reaction Times of Aimed Movements: Effects of Practice, Uncertainty, and Change in Target Location" by A. P. Georgopoulos, J. F. Kalaska, and J. T. Massey, 1981, *Journal of Neurophysiology, 46,* 725–743. Copyright 1981 by the American Physiological Society. Reprinted by permission.

that interacts with the controlled plant. Separate circuitry for separate targets, perturbed targets, or different durations is unnecessary. Rather, the single model produces trajectories parameterized by target location and duration. It is notable that duration is an input to this model, rather than an emergent quantity. Movement duration is dependent on, among other parameters, distance moved and the timing, distance, and direction of target perturbation. This dependency is the subject of another model, presented in Hoff (1992), which reproduces unperturbed and perturbed durations for three of the bodies of experimental data addressed in this article.

Flash and Henis (1992) found that a particular body of kinematic reaching data was reproduced better by a partially overlapping superposition of two minimum-jerk trajectories than by a sequence of two minimum-jerk trajectories, such as the one modeled in this section. We acknowledge their results, while maintaining the applicability of the model presented here for reproducing the data as shown in this section, for providing a plausible and robust trajectory-generation mechanism, and for providing a basis for modeling both reach and prehension, as shown in the following section.

3. Modeling the Cooperative Interaction of Reach and Grasp in Prehension

The time has come to review recent experimental work that refined the view of the interaction of arm and hand movements presented in Figure 1a and to develop the new model of this interaction hinted at in Figure 1b. Section 3.1 introduces the body of experimental data to be addressed. Section 3.2 discusses details of the experimental results of the interaction of transport and preshape, along with their impact on the formation of the model. Section 3.3 presents simulation results of the combined optimal control kinematic models of transport and preshape, with synchronization based on the described timing principles. Appendices A and B describe in detail the mathematical derivations behind the results presented here.

3.1 Investigations of Hand Transport and Preshape Interaction

Paulignan, MacKenzie, et al. (1991) had subjects reach to grasp a dowel located in the horizontal plane, 35 cm from the hand, in a direction 20° to the right of the mid-sagittal plane. In certain trials, the location was unexpectedly shifted, at movement onset, to a second target located either 10° (leftward) or 30° (rightward) from the mid-sagittal plane. Perturbation of location had an effect not only on transport of the hand (which corrected to reach the new target), but also on the kinematics and timing of preshape: Maximum *aperture* (the separation of the thumb and forefinger) was found to occur later in the movement, after the hand temporarily closed to a smaller aperture.

Gentilucci, Chieffi, Scarpa, and Castiello (1992) performed a location-perturbation prehension experiment, in which subjects reached to grasp one of three 4-cm diameter spheres positioned on a table 15, 27.5, and 40 cm from the hand's starting position. During some of the trials, while subjects reached to the nearest sphere, a switch was made to one of the more distant ones. Kinematics of hand movement and finger preshape were recorded to determine the effect of target distance and perturbation on subject performance.

Paulignan, Jeannerod, MacKenzie, and Marteniuk (1991) had subjects reach and grasp dowels of diameters 1.5 cm and 6 cm, and perturbed the target size by switching the dowels at movement onset, both from small to large and large to small. In the perturbation trials, as the hand took additional time to reach the correct aperture, its transport slowed to reach the object at an appropriately later time.

We now turn to the interpretation of these findings and their integration into a cohesive computational model.

3.2 Modeling Transport and Preshape Interaction

Temporal Interaction of Transport and Preshape

In the position-perturbation trials of Paulignan, MacKenzie, et al. (1991), a kinematic response was seen within 100 ms,[4] in the form of an early peak in acceleration. Using Δ_L to represent the sensorimotor delay from location perturbation to response in the hand transport process, we can set an upper bound of $\Delta_L \leq 100$ ms. The movement time for the unperturbed task averaged 510 ms and was lengthened by location perturbation: On the average, perturbed-left (PL) movements were lengthened by 80 ms whereas perturbed-right (PR) movements were lengthened by 112 ms. In the unperturbed case, as the hand preshaped, the maximum hand aperture was attained at 323 ms. After target-location perturbation, there was an abbreviated aperture peak (202 ms PL, 232 ms PR) followed by a new maximum aperture (420 ms PL, 446 ms PR). This early aperture peak puts an upper bound of about 200 ms on the reaction time of preshape to location perturbation. Thus, if we use Δ_{LP} to represent the increased delay for the preshape motor process to respond to location perturbation beyond the delay Δ_L, then we can state this upper bound as $\Delta_{LP} + \Delta_L \leq 200$ ms. Note also that movement duration minus time to second peak aperture was consistent (170 ms PL, 176 ms PR). In the unperturbed case, this difference was 187 ms. Possibly the maximum aperture is synchronized with the end of the reaching movement so that interaction with the object to be grasped can be controlled, with coordination based on keeping consistent the *enclose time* (*ET*), the difference between the time at which the movement ends and the time at which the hand achieves maximum aperture.

When unperturbed, object size had little effect on reaching kinematics or movement time, which was similar to the control for the target-perturbation paradigm (Paulignan, Jeannerod, et al., 1991). The difference between end of movement and maximum aperture was consistent with the earlier experiments: 199 ms (S), 187 ms (L). Object size did, of course, effect the magnitude of peak aperture, which

was 9.2 cm (S), or 12.5 cm (L). In the small-to-large perturbation (S-L) case, movement time increased by 175 ms on the average. The increase was all in the low-velocity phase, because the earlier kinematic landmarks (maximum velocity, maximum deceleration) did not change. In three subjects, two peaks were observed in hand aperture. The first peak occurred slightly earlier (294 ms) than in the unperturbed small target preshape (309 ms). (Note that this implies that reaction time of preshape to size change is less than or equal to 294 ms. We may introduce Δ_S as this time delay and restate the upper bound as $\Delta_S \leq 294$ ms.) The second peak had amplitude corresponding to the large target (12.2 cm), as expected, and occurred 475 ms after movement onset. The transition between the two peaks can be identified by the time when the rate of change of aperture became zero, at 330 ms. In the other two subjects, there was only an inflexion at the transition point; there were not two distinct peaks. Because movement time increased to 684 ms in response to the small-to-large perturbation, *ET* in (S-L) was 209 ms.

Large-to-small perturbation (L-S) caused an increase in movement time of 85 ms. As in the S-L perturbation, the transport kinematics before maximum deceleration were unchanged. Thus the transport reaction time to the size perturbation was longer than the time to peak deceleration, about 300 ms. We introduce $\Delta_S + \Delta_{ST}$ as this time delay and restate the lower bound, $\Delta_S \pm \Delta_{ST} \geq 300$ ms. The aperture trajectory typically showed only a single peak: The enclosure phase was prolonged until the small dowel aperture size was reached.

In the enclose-time studies of Gentilucci et al. (1992), *ET* was, again, approximately 200 ms, corroborating the results of Paulignan, MacKenzie, et al. (1991). Although movement time, time to maximum aperture, and other kinematic landmarks varied with distance and perturbation, the enclose time was found to be consistent throughout. It would seem the central nervous system (CNS) coordinates transport and grasp to allow the hand 200 ms to close on the target; the closure coincides with the movement's end.

To formally check whether *ET* varies with perturbation, we examined the data (provided by the Jeannerod laboratory, from the experiments reported in Paulignan, MacKenzie, et al., 1991) from 56 unperturbed trials, 48 perturbed left, and 56 perturbed right. The mean enclose time was 180.9 ms. For the unperturbed trials, *ET* was 185.4 ms; for PL, it was 177.4 ms; and for PR, it was 179.3 ms. Thus *ET* varied very little due to perturbation, compared with the changes in other temporal variables, such as movement time. We performed an analysis of variance (ANOVA) on the *ET* data to show that, at the 99% confidence level, *ET* did not significantly vary between the three conditions.

It is now appropriate to introduce the *constant enclose-time* model embodied in Figure 5. Following the schematic approach in the coordinated control program of Figure 1, we have motor activity generators (the transport, preshape, and enclose controllers) that take as input target position values and planned movement durations. The transport trajectory generator takes as input target location and duration (the allocated time for the movement). The inputs for the preshape trajectory generator are maximum aperture (itself a function of object size) and duration. Object location and size provide hypothesized duration estimation modules (the boxes labeled *transport time needed* and *preshape time needed*) with information for independent judgments of the time necessary for each process. Although the modules are dependent on experimental parameters, the present model simply used empirical data to approximate their output. These estimates interact through the elements labeled *MAX* so that the maximum of transport time needed and preshape time needed plus enclose time needed (the input *ET* is the desired enclose time for the grip, as discussed earlier) is fed to the trajectory-generation schemas. The result is that the two processes are each scaled to the longer duration. After this time is determined, *ET* is subtracted from the duration determined by the MAX comparators and the result is sent to the preshape controller. Thus, the hand preshape will always reach its target maximum aperture prior to the transport position's reaching its target, and the amount of the lead will be the time needed for closure.

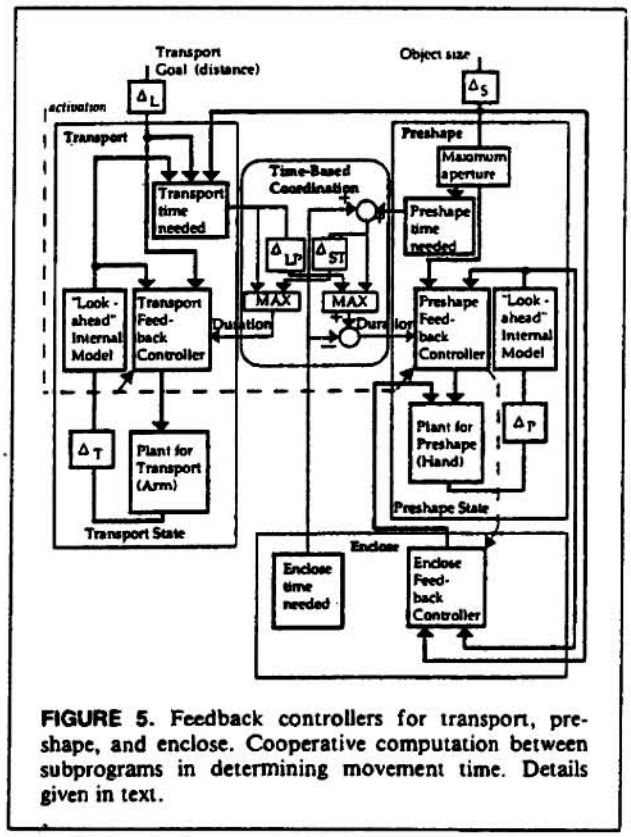

FIGURE 5. Feedback controllers for transport, preshape, and enclose. Cooperative computation between subprograms in determining movement time. Details given in text.

It is important to emphasize that the constant enclose-time model does not claim that hand enclose time is constant across all object sizes and grip types; rather, it says that enclose time is constant across perturbation situations for a particular task. In Section 4, we will turn to the sub-

ject of how object size, as an example of one of many relevant factors, affects enclose time.

The pathways along which spatial and temporal data are passed have intrinsic delays, shown in Figure 5, some values of which we have already discussed. Further, Δ_T and Δ_P are the lumped sensorimotor feedback delays for transport and preshape, respectively, as introduced in Section 2.2 for the model of reach control. The enclose controller is, in the model, identical to the preshape controller, but with different inputs: Its duration is *ET*, and its target value is the object size, rather than the larger maximum aperture. Thus, it has the function of closing the hand to the object size at the end of the movement time. The planned movement duration for each controller is presented in the form of the *time remaining* for the movement, and as such it constantly decreases, once the movement begins, until reaching zero.

The box labeled *maximum aperture* performs a mapping from object size to the maximum aperture of the grip. From the two object sizes in Paulignan, Jeannerod, et al. (1991), we generate the linear mapping,

$$Max\ Ap = .75*Dowel\ Diameter + 4.55\ \text{cm},$$

which is consistent with the findings of Marteniuk, Leavitt, MacKenzie, and Athenes (1990), who had subjects reach to grasp disks of various sizes (5.5 to 12.5 cm in diameter) and derived the relationship $Max\ Ap = .77*Disk\ Size + 4.89$ cm.

Trajectory Generation for Transport and Prehension

In formulating the movement controllers for transport and prehension, we retained the controller described in Section 2.2 for transport. The extension of the controller from a one-dimensional plant to multiple dimensions was straightforward (Flash & Hogan, 1985). The significant addition was a change in the final end-point constraint to allow control of the hand orientation as the target is approached (see Appendix A). For the preshape formation controller, we searched for the simplest cost function that captures the characteristics of the movement kinematics. As with any continuous system, some smoothness criterion is needed to prevent discontinuous jumps in the resulting trajectory. Next, the partial reclosing of the hand during prolonged movement caused by location perturbation implies that there is some cost to having the hand open more than a certain amount. The relative importance of these two criteria is not known a priori, so a weighting parameter was introduced, yielding the following criterion for preshape:

$$J = \int_0^{t_f} \{x(t)^2 + w[d^2x(t)/dt^2]^2\}dt, \qquad (5)$$

where $x(t)$ is the hand's aperture, and w is the relative weighting of the two components and is tuned empirically. This cost criterion is used both for preshape and enclose, under the assumption that the same neural control system drives the fingers in each case. The difference is the inputs to the controller for enclose: The target hand aperture is the object size, whereas the allocated time is simply the enclose time.

To find the trajectories associated with the above optimization criterion, it is necessary to know the onset of movement ($t = 0$), along with the duration ($t = t_f$). Boundary conditions on the system state (e.g., the initial and final values for the aperture of the hand, the location of the target, and the hand's approach direction) must also be known. In addition, any weighting parameters must be determined. In this case, the only parameter is w in the preshape criterion. We will discuss how this was empirically determined. Given these parameters, we employed the maximum principle (Takahashi, Rabins, & Auslander, 1970) to derive an optimal trajectory of the system's state based on the optimization criterion and the system's dynamics. The details of this derivation are given in Appendix B.

3.3 Simulation of the Transport/Prehension Model

We created a computer simulation of the elements shown in Figure 5 to test the model against experimental data. The inputs to the simulation were object location and size, optionally modified during the simulation to reflect perturbations. The graphic output of the simulation shows the kinematics of reach and preshape during the task. Position and velocity of the hand are shown for the x and y components. In addition, the resultant magnitudes of position and velocity were plotted, for comparison with actual data. An $x - y$ plot of the hand's path with one point for each simulation time step gives a useful visualization of the combined transport data. The time course of the hand's aperture during preshape was plotted as well as its derivative.

Simulating Perturbed Location and Size

We begin by reproducing the results of Paulignan, MacKenzie, et al. (1991) and then show how the simulation can be used to reproduce other bodies of data. Following the review in Section 3.2, we set the transport time needed in the simulation to 510 ms, and the preshape time needed to 310 ms. (We did this because the model says that the movement time—510 ms—is the maximum of the transport time needed and the sum of the preshape time needed and the enclose time. The outcome will be the same if either the former or the latter time-needed value is lowered.) We assigned Δ_L the value of 100 ms based on the timing of location-perturbation reaction. Δ_{LP} is the preshape response latency to location perturbation (200 ms) minus Δ_L; thus it was set to 100 ms. The target approach orientation parameter ϕ (see Appendix A), was set to 90°, the direction directly away from the subject. The coordinates of the target wrist position were set to (2 cm, 24 cm). Figure 6 shows the kinematics of transport and prehension for unperturbed movement to the center target to grasp the small target. Figures 6a, c, and e show actual data, whereas b, d, and f show simulation results. Figure 6a shows the path of the wrist during unperturbed reach and grasp of a central dowel. Figure 6b shows the simulation of an unperturbed wrist path when reaching toward the center target. (The left and right

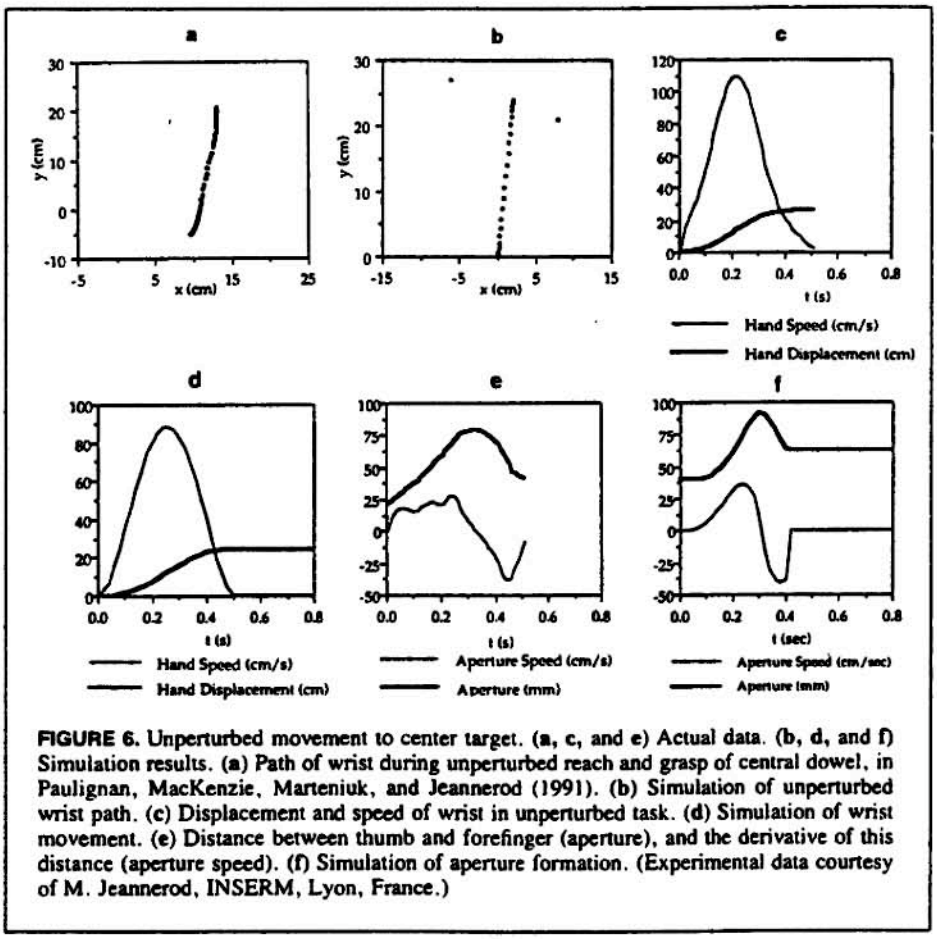

FIGURE 6. Unperturbed movement to center target. (**a**, **c**, and **e**) Actual data. (**b**, **d**, and **f**) Simulation results. (**a**) Path of wrist during unperturbed reach and grasp of central dowel, in Paulignan, MacKenzie, Marteniuk, and Jeannerod (1991). (**b**) Simulation of unperturbed wrist path. (**c**) Displacement and speed of wrist in unperturbed task. (**d**) Simulation of wrist movement. (**e**) Distance between thumb and forefinger (aperture), and the derivative of this distance (aperture speed). (**f**) Simulation of aperture formation. (Experimental data courtesy of M. Jeannerod, INSERM, Lyon, France.)

target locations are also shown.) Figure 6c shows displacement and wrist speed in the unperturbed task. Figure 6f shows the simulation of wrist movement. Figure 6e shows distance between thumb and forefinger (aperture), and the derivative of this distance (aperture speed). Figure 6f shows the simulation of aperture formation. Because the minimum-jerk cost functional was used, the simulated hand path and velocity profile of Figures 6b and 6d captured the roughly straight wrist movement and single-peak velocity profile, seen in the data. The aperture formation model was able to capture the amplitude and timing of peak aperture, as well as the enclose time, seen in the data, Figure 6e. Simulation parameters included the initial aperture (which reflects the offset of IRED markers from the fingers) of 4 cm, and the two object diameters, 6.2 cm and 1.6 cm. The model predicted a slightly faster opening phase (Figure 6f) than was evident in the data, whereas the closing phase velocity was accurately reproduced. To model higher-order derivatives in the trajectory, we would need to introduce models more detailed than that described by Equation 5. Our goal here was to capture the timing and amplitude of the aperture itself, under normal and perturbed conditions, using the simplest possible model. We now turn our attention to the perturbed conditions.

For target-location perturbation, right or left, transport time needed in the model was increased by 100 ms, again following the data in Section 3.2. The coordinates of the target wrist locations were set to (-6 cm, 27 cm) and (8 cm, 21 cm) for the left and right targets, respectively. Figure 7 shows the data and simulation results for the perturbed-left case. When target location was perturbed, transport had a corrective trajectory, following a velocity peak at about 200 ms, and prolonged deceleration phase. Note that the target approach direction was maintained despite target location perturbation (due to the terminal orientation constraint on the modeled hand path). The simulated aperture trajectory shown in Figure 7f exhibits the temporary reclosing seen in the recorded trajectory during location perturbation (Figure 7e). The local minimum in the aperture was 25 mm less than the final peak aperture in both the data and simulation. The double sequence of acceleration followed by deceleration seen in the aperture velocity profile of Figure 7e was also reproduced by the simulation.

For target size perturbation, transport time needed was increased by 175 ms for S-L and 100 ms for L-S, following the empirical data. The values of Δ_s and w were set experimentally, observing simulated preshape profiles for each combination. Values of Δ_s from very low, 100 ms, to the

upper bound, 294 ms, were entered into the model. w serves as a time constant in the preshape function, controlling the sharpness of the response of the preshape profile to shifting target aperture. The simulation parameter Pwt was equal to $\sqrt{2}w^{1/4}$, and for values below .10 gave realistic preshape trajectories. Values from .05 to .10 were tried in combination with the values of Δ_s above in normal and perturbed simulations, observing peak aperture velocity, timing of perturbation response, and general similarity in shape to experimental curves. The values that gave the best fit were Δ_s = 250 ms and Pwt = .09. To give the empirical value of 300 ms to the timing of transport's response to change in object size, we assigned to Δ_{ST} the remaining 50 ms.

Figure 8 shows the data and simulation results for the case in which the target size was unexpectedly increased, whereas Figure 9 shows the case where the target size was unexpectedly decreased. As expected, the preshape process made an on-line correction to a larger aperture, seen in Figure 8d as well as in Figure 8c. The model yielded a quantitatively correct reconstruction of aperture formation: As in the data, the simulated aperture leveled off at about 90 mm, 300 ms after movement began, then proceeded to the larger aperture, 120 mm, reaching it at 475 ms. The aperture derivative had two peaks, corresponding to each *opening phase* in the aperture development, but the magnitudes in the simulation did not correspond with the magnitudes in the data. Again, the simple model chosen here captured the essential features of aperture formation. To capture features of higher-order derivatives in the trajectory, a more detailed model is needed. The effect of size perturbation on transport was qualitatively reproduced: The later part of transport (the deceleration phase) appears prolonged in Figure 8b as in 8a, slowing to synchronize with the preshape process. In Figure 9a and b, the effect on transport was a similar slowing. In Figure 9c and d, the enclosing hand, after peaking at 320 ms at or near the unperturbed peak aperture of 120 mm, switched smoothly to a smaller peak aperture and continued into the enclose phase. In Figure 8a and b and 9a and b, the timing of peak velocity was not affected by size perturbation, because the peak occurred prior to the delayed effect of size perturbation on transport. Paulignan, Jeannerod, et al. (1991) found that in the unperturbed case maximum hand velocity occurred around 185 ms for both unperturbed reach to the small and large objects, and for both size perturbation cases (Figures 8a, 9a). The simulations reflected this consistency in time to peak velocity (Figures 8b, 9b).

Simulating Jeannerod (1981)

Jeannerod (1981) recorded kinematics of transport, preshape, and grasp to targets of varying sizes, and during target size perturbation. Subjects reached to grasp a target object placed on a tabletop, then put the object in a small box.

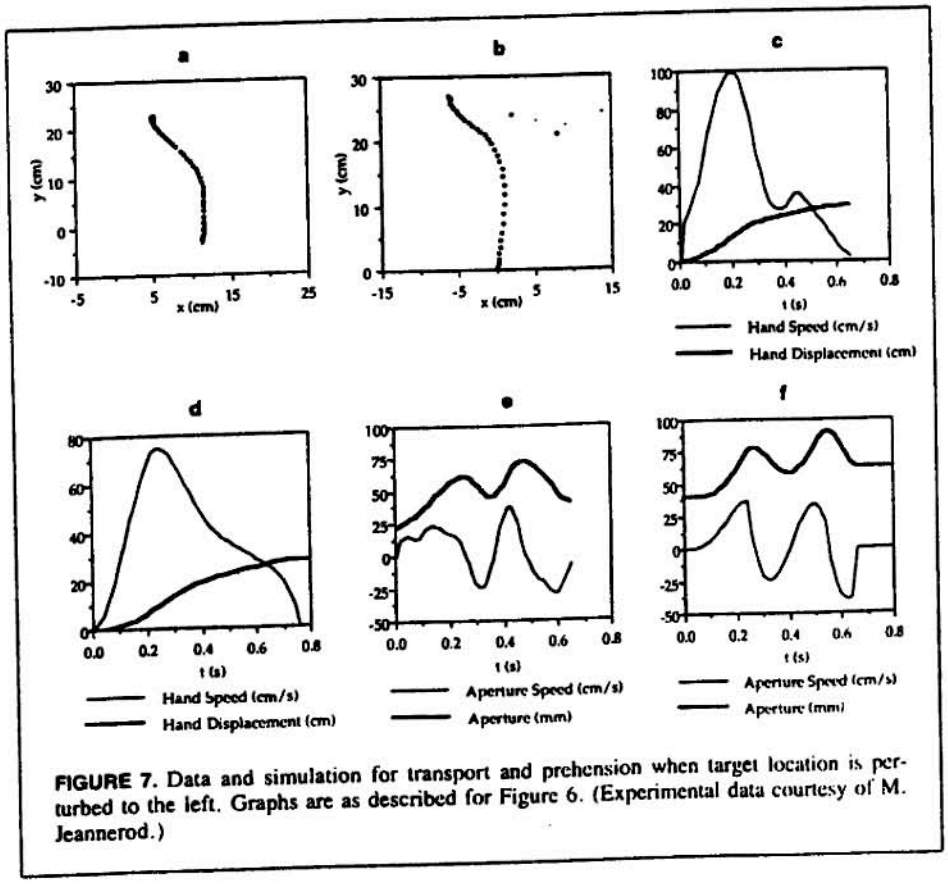

FIGURE 7. Data and simulation for transport and prehension when target location is perturbed to the left. Graphs are as described for Figure 6. (Experimental data courtesy of M. Jeannerod.)

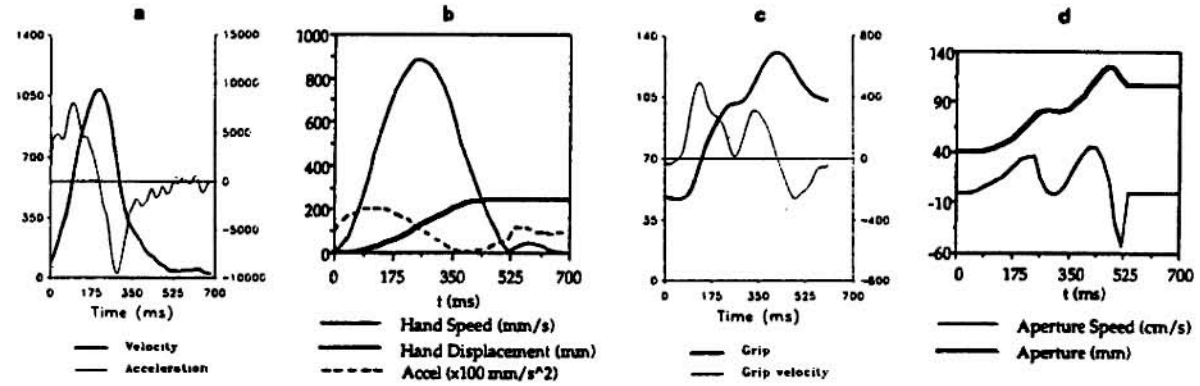

FIGURE 8. Data and simulation for transport and prehension when target size is unexpectedly increased (S-L). (a,c,) Actual data. (b,d) Simulation results. (a) Speed (scale is left vertical axis, in mm/s) and acceleration (scale is right vertical axis, in mm/s^2) of wrist in S-L task (Paulignan, Jeannerod, MacKenzie, & Marteniuk, 1991). (b) Simulation of wrist movement. (c) Aperture (scale is left vertical axis, in mm) and its derivative (scale is right vertical axis, in mm/s) in the S-L task. (d) Simulation of aperture formation. (Experimental data courtesy of M. Jeannerod.) *Note.* Parts a and c are from "Selective Perturbation of Visual Input During Prehension Movements. 2. The Effects of Changing Object Size" by Y. Paulignan, M. Jeannerod, C. MacKenzie, and R. Marteniuk, 1991, *Experimental Brain Research, 87,* 407–420. Copyright 1981 by Springer-Verlag Publishers. Reprinted by permission.

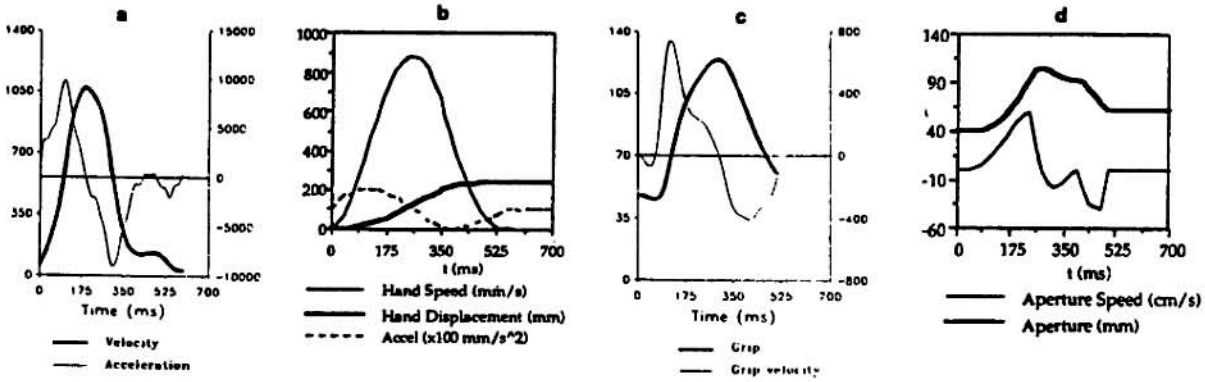

FIGURE 9. Data and simulation for transport and prehension when target size is unexpectedly decreased. Graphs are as described for Figure 8. (Experimental data courtesy of M. Jeannerod.) *Note.* Parts a and c are from "Selective Perturbation of Visual Input During Prehension Movements. 2. The Effects of Changing Object Size" by Y. Paulignan, M. Jeannerod, C. MacKenzie, and R. Marteniuk, 1991, *Experimental Brain Research, 87,* 407–420. Copyright 1981 by Springer-Verlag Publishers. Reprinted by permission.

In one experiment, the object was a sphere that could be suddenly modified in apparent size, between 4 and 7 cm in diameter. The size change was produced at movement initiation. Perturbation of object size affected the formation of grip by the fingers but not the transport of the hand. The timing and magnitude of various kinematic landmarks were unaffected by perturbation. Movement time was typically 800 ms in both normal trials and perturbed trials.

We wished to test whether our model of transport/preshape interdependence could also address these findings. In S-L size perturbation simulation discussed previously, the *movement-time-needed* parameter was changed from 510 ms to 800 ms, reflecting the slower movement encountered in Jeannerod's study. The object sizes were modified in correspondence with the values given for the experiment. Results are shown in Figure 10 for simulated reaches to unperturbed (Figure 10a and b) and perturbed (Figure 10c and d) targets. (Graphs of transport and preshape trajectories from the original experiment were unavailable. We show the simulated trajectories not for direct comparison, but to illustrate the response of each process in the model to the perturbation.) Note that despite the size perturbation, additional time was not needed, because the adjusted preshape fit within the limits of the transport movement time. Spe-

cifically, in the MAX comparator shown in Figure 5, the duration sent to the transport controller was 800 ms both before and after object size perturbation. Before perturbation, the movement time needed (800 ms) was compared with the preshape time needed plus the enclose time (310 ms + 200 ms = 510 ms), and the maximum was 800 ms. After perturbation, the preshape time needed increased by 175 ms; so the sum of preshape and enclose time became 685 ms. This still was dominated by the slower movement time, however; so the maximum remained 800 ms, and transport was unaffected by the perturbation. The model predicts that only for movement durations under about 685 ms will size perturbation affect overall movement time.

Predictions of the Model

Toward testing the predictive ability of the model described, we simulated a novel variation on the prehension task studied in the above experiments. In particular, we wondered what the effect would be of asking a subject to grasp an object very near to her hand, under a tight time constraint. Thus the transport process would, if unconstrained by the prehension process, operate very quickly. To simulate this, we set, in the simulation, the transport-time-needed parameter to 200 ms and the movement distance to 2 cm. The results are shown in Figure 11. Because the time needed by the transport process was much less than that needed by the preshape and enclose processes, the movement time was dictated by the latter. Thus transport was extended in time to match the hand's movement, resulting in the low-velocity profile seen in Figure 11a. The model used in this article predicts that in general, for short reaching movements, there is a lower bound on the movement time when there is an associated grasping task. Further, as noted in the discussion on the simulation of the experiments of Paulignan, MacKenzie, et al. (1991), although we assumed the preshape time needed was 310 ms, this was actually an upper bound on its value. In may be that the transport time needed is dominant, overriding a shorter enclose time. By performing the task described here, an experimenter would reveal the true preshape-time-needed value, because it presumably would be the limiting time factor in the overall movement.

The maximum comparison (MAX) element of this model predicts that duration extensions caused by location and size perturbations do not sum; rather, the maximum is taken. Figure 12 shows results of simulating a movement with simultaneous perturbation of both target location and size. At the onset of movement, the target was both shifted to the right and enlarged, using the target locations from Paulignan, MacKenzie, et al. (1991) and sizes from Paulignan, Jeannerod, et al. (1991). Because the increased movement times for leftward perturbation (100 ms) and for increased object size (175 ms) overlapped instead of summing, the total movement time increase was 175 ms, the larger of the two changes.

4. Discussion

We have expanded an existing schema model of the interaction between reach and grasp to give an account at the kinematic level, appropriate for comparing against the output of behavioral experiments. We have built upon the minimum-jerk trajectory-formation model to posit a control model that reflects the consequences of sensory input and motor correction during movement. Thus the formulation incorporates the features and kinematic realism of the original minimum-jerk model, while expanding the paradigm to model movements during target perturbation.

The two dimensional (2-D) minimum-jerk model was further modified to address a constraint on the terminal path direction, which is present in reaching-to-grasp movements, but not necessarily present in nonmanipulative arm movements such as reaching to point. The result is intuitively acceptable: Task constraints applicable to the trajectory's end (e.g., the approach direction of an object to be grasped) affect kinematics during the reach. Thus the reach is planned with respect to the overall goal of the movement.

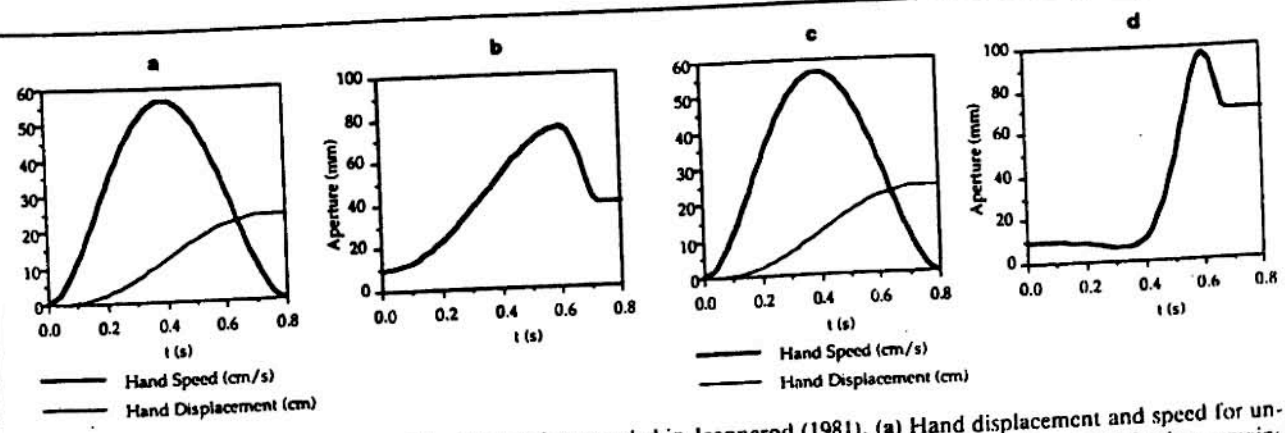

FIGURE 10. Results for replication of the kinematics recorded in Jeannerod (1981). (a) Hand displacement and speed for unperturbed reach. (b) Hand aperture for unperturbed reach. (c) Hand trajectory for perturbed case. Movement in time remains 800 ms. (d) Hand aperture for perturbed case.

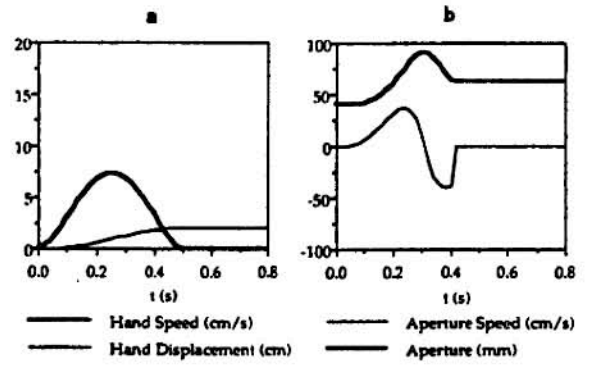

FIGURE 11. Results of simulating a short, quick movement. (a) Wrist movement. (b) Hand aperture formation. Because aperture formation is the limiting factor in the movement, transport slows to match it temporally, resulting in a low peak wrist velocity.

as seen when reaching occurs under varying accuracy constraints (e.g., Milner & Ijaz, 1990). In a similar vein, the constant enclose-time model for the timing of reach and grasp implies that the nervous system starts from the constraints of object interaction (i.e., the hand's enclose time) and then plans the preceding segments of the motor task (transport and preshape) in accordance with these constraints.

Lastly, the model of the interaction of reach and grasp embodies what is seen in perturbation studies: that there is not a strict hierarchy of the two processes. Rather, as external factors change the activity of either process, one may, in turn, influence the activity of the other.

Comments on the Maximum Duration Model

Regarding the temporal interaction model of Section 3, there are other examples of motor control processes where temporal coordination is produced by slowing or delaying a process that otherwise would be quicker. In oculomotor control, it is known that although there are separate brain stem centers for generating vertical and horizontal saccade components, an oblique saccade is characterized by a roughly straight movement of the pupil. If both components proceeded at maximum speed and the saccade direction was other than 45°, the shorter component would finish first, causing an abrupt discontinuity in the movement direction. Instead, it has been observed that the shorter component is sufficiently slowed in its progression that the two components terminate together (Fuchs, Kaneko, & Scudder, 1985). Rogal and Fischer (1986) found that for combined eye and arm movement, saccade and reach were prepared in parallel, but if the saccade preparation time exceeded that of reach, then reach execution was delayed. This resulted in higher correlation between reach and saccade onset times when saccade preparation was made to be very time consuming. Thus, in this example, it was the preparation times of two processes that were synchronized in their duration.

Observations on Enclose Time

Earlier, we discussed the lack of an effect of perturbation on enclose time (*ET*). This motivated consistency of *ET* as a model of motor task coordination. Although *ET* for the hand during grasp is hypothesized to be invariant under perturbation, *ET* certainly is not invariant across all grasping tasks. In Marteniuk et al. (1990), different sized disks were grasped by human subjects. The disks varied in diameter (*DIA*) from 1 cm to 10 cm. It was found that as disk size decreased, movement time (*MT*) increased (as predicted by the speed/accuracy trade-off), but also the time to peak aperture (*TPA*) decreased. The relationship between *TPA* and *DIA* in their data is summarized by the least squares fit linear relationship,

$$TPA = 491 \text{ ms} + DIA\ 6.10 \text{ ms/cm}.$$

Similarly, *MT* is related to *DIA* by

$$MT = 681 \text{ ms} - DIA\ 5.94 \text{ ms/cm}.$$

Because $ET = MT - TPA$, the relationship between *ET* and *DIA* is given by

$$ET = 190 \text{ ms} - DIA\ 12.04 \text{ ms/cm}.$$

Thus enclose time increases as disk size decreases. There are two interpretations of this. First, the hand physically needs more time to close to a smaller size. Second, there may be a speed/accuracy trade-off for grasping as well as for reaching. This relationship between *DIA* and *ET* predicts $ET = 172$ ms for a disk of diameter 1.5 cm. This is in the ballpark of the *ET* seen in Paulignan, MacKenzie, et al. (1991). For a disk of size 6 cm, however, the predicted *ET* is 118 ms; whereas in Paulignan, Jeannerod, et al. (1991), the average enclose time for the 6-cm diameter dowel was 187 ms. There may be other factors (disk height, experimental set-up) that contributed to the discrepancy between *ET* in the two experiments. Further investigation is needed to isolate the responsible factors.

New Experiments

The goal of the modeling work in this article was to stimulate further experimentation. With the simulation of imagined experiments in Section 3.3 we hope to inspire novel variations on the behavioral experiments already performed, both to test and refine the model presented here. Specifically, the testable hypotheses are (a) that there is a lower bound on movement time, dictated by the prehension process, which limits the speed of transport, and (b) that simultaneous perturbation of size and location of a reaching target will not slow the action by the sum of the individual delays, but by the maximum of the two. Further, the application of the model to the data of Jeannerod (1981) suggests that there is a maximum movement time for which object size perturbation will slow the movement, that maximum being 685 ms.

In the transport and prehension model, the outputs of the two maps labeled *transport time needed* and *preshape time*

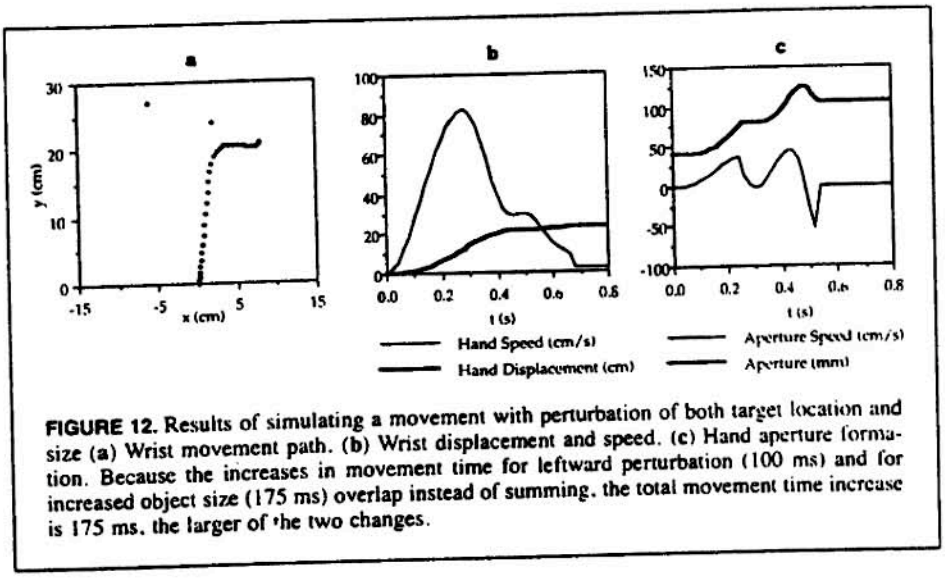

FIGURE 12. Results of simulating a movement with perturbation of both target location and size (a) Wrist movement path. (b) Wrist displacement and speed. (c) Hand aperture formation. Because the increases in movement time for leftward perturbation (100 ms) and for increased object size (175 ms) overlap instead of summing, the total movement time increase is 175 ms, the larger of the two changes.

needed were set empirically, based on the data. In reality, they are dependent on target location and size, as well as time, magnitude, and direction of perturbation. The experimental data only sparsely sampled the parameter space. To clearly elucidate the dependency of the time-needed maps' outputs on the various experimental inputs, further experiments are needed in which a greater variety of these parameters are utilized.

APPENDIX A

The Use of Optimal Control to Derive Transport Trajectories

Let the system being controlled be described by

$$x_i' = f_i(x, u), \qquad i = 1 \text{ to } n,$$

where x is the system's state variable vector and $u = (u_1, \ldots, u_m)$ is the control vector. For the one-dimensional minimum-jerk model, the dynamic system to be controlled is

$$x_1' = x_2,$$

$$x_2' = x_3,$$

$$x_3' = u,$$

where x_1 represents position, x_2 represents velocity, x_3 represents acceleration, and the input u is the jerk (derivative of acceleration). Hogan (1984) and Flash and Hogan (1985) have shown that, for the minimum-jerk optimization criterion,

$$J = \int_0^{t_f} u^2 dt, \tag{A.1}$$

the optimum position trajectory, $x_1(t)$, is a quintic function of time. Therefore, its second derivative, the acceleration $x_3(t)$, is a cubic function of time. The coefficients of these polynomials are determined from the boundary conditions: the system's initial and final states. The initial state is given as a 3-tuple of position, velocity, and acceleration: $(x_1^i, x_2^i, x_3^i)^T$. The final state is $(x_1^f, 0, 0)^T$, where the zeros indicate a static state. Applying these boundary conditions to the system yields, for the acceleration,

$$\begin{aligned} x_3(t) = {} & x_3^i[1 - 9\tau + 18\tau^2 - 10\tau^3] \\ & + x_2^i[-36\tau + 96\tau^2 - 60\tau^3]/D \\ & + (x_1^f - x_1^i)[60\tau - 180\tau^2 + 120\tau^3]/D^2, \end{aligned} \tag{A.2}$$

where the movement begins at $t = t_i$ and ends at $t = t_f$, so that $D = t_f - t_i$ is the duration and $\tau = (t - t_i)/D$ is a normalized time variable. Equation A.2 is the same as Equation 1, which is used to design the controller for trajectory generation in the one-dimensional reach model.

Flash and Hogan (1985) showed that for a two-dimensional (2-D) system, the dimensions of movement are decoupled and the trajectory in each dimension is a quintic polynomial, as in the 1-D case. To implement the control of the 2-D system according to the specified optimization criterion, it is necessary only to have two uncoupled controllers for each dimension, each identical to that for the 1-D case, derived earlier.

In the 2-D system, we may control the orientation of the hand at the trajectory's end, as well as its position. In the 1-D system, we had three boundary conditions at the final time, one for each component of the final state. We specified that the final state be static (have zero velocity and acceleration) and be located at the target $(x_1^f, 0, 0)^T$. The extension to two dimensions provides for six final-time conditions. Let x_1, x_2, and x_3 represent, respectively, the position, velocity, and acceleration in the first dimension, and x_4, x_5, and x_6 represent, respectively, the position, velocity, and acceleration in the second dimension. In choosing the final-time conditions, because we wish the target position to be reached, we specify

$$x_1(t_f) = x_1^f, \qquad x_4(t_f) = x_4^f, \tag{A.3}$$

where the target is located at (x_1^f, x_4^f). Because the final position is to be static, we specify that the velocity of each component be zero,

$$x_2(t_f) = 0, \qquad x_5(t_f) = 0. \tag{A.4}$$

We also want the target to be approached from a specific angle: Figure 7a shows a wrist trajectory that approaches from the direction of the subject. Intuitively, this is necessary because the hand must approach with the finger aperture facing the target. The most comfortable posture for one's hand in this experimental paradigm is with the fingers facing away, thus target approach is typically

from the subject's side of the target. We capture this phenomenon by specifying the following fifth boundary condition:

$$\lim_{t \to t_f} \frac{x_1(t) - x_1^f}{x_4(t) - x_4^f} = \phi, \tag{A.5}$$

where ϕ is the slope of the trajectory (in the horizontal plane) during approach. Now because (A.3) holds, this is the ratio of vanishingly small quantities and cannot be evaluated in its given form. Instead, we apply l'Hopital's rule and differentiate the numerator and denominator, obtaining

$$\phi = \lim_{t \to t_f} \frac{x_1(t) - x_1^f}{x_4(t) - x_4^f} = \lim_{t \to t_f} \frac{\left(x_1(t) - x_1^f\right)'}{\left(x_4(t) - x_4^f\right)'},$$

$$\phi = \lim_{t \to t_f} \frac{x_1'(t) - 0}{x_4'(t) - 0} = \lim_{t \to t_f} \frac{x_2(t)}{x_5(t)}.$$

Now, from (A.4), this too is a ratio of vanishingly small quantities; thus we differentiate once more.

$$\phi = \lim_{t \to t_f} \frac{x_2'(t)}{x_5'(t)} = \lim_{t \to t_f} \frac{x_3(t)}{x_6(t)},$$

or

$$\phi = \frac{x_3(t_f)}{x_6(t_f)}. \tag{A.6}$$

Thus the fifth constraint is equivalent to our fixing the ratio of the terminal acceleration values. The sixth constraint is the magnitude of one of the terminal acceleration values (with Equation A.6 determining the magnitude of the other). This magnitude is a free parameter of the simulation chosen to best fit the experimental data. (In our simulations, we found that the best fit to the data was generated with $x_6^f = -5$ m/s^2.) We can write these two constraints as

$$x_6(t_f) = x_6^f, \qquad 3(t_f) = \phi\, x_6^f.$$

Making the appropriate extension to Equation A.2 for non-zero final acceleration, and applying these boundary conditions, we have

$$\begin{aligned} x_3(t) = {} & x_3^o\,[1 - 9\tau + 18\tau^2 - 10\tau^3] \\ & + \phi x_6^f[3\tau - 12\tau^2 + 10\tau^3] \\ & + x_2^o\,[-36\tau + 96\tau^2 - 60\tau^3]/D \\ & + (x_1^f - x_1^o)[60\tau - 180\tau^2 + 120\tau^3]/D^2, \end{aligned}$$

$$\begin{aligned} x_6(t) = {} & x_6^o[1 - 9\tau + 18\tau^2 - 10\tau^3] \\ & + x_6^f[3\tau - 12\tau^2 + 10\tau^3] \\ & + x_5^o[-36\tau + 96\tau^2 - 60\tau^3]/D \\ & + (x_4^f - x_4^o)[60\tau - 180\tau^2 + 120\tau^3]/D^2, \end{aligned}$$

which then are used, as was (A.2) in Section 2.2, to construct the 2-D transport controller.

APPENDIX B

The Use of Optimal Control to Derive Preshape Trajectories

Trajectory optimization may be achieved by using the maximum principle, which, as described by Takahashi et al. (1970), applies to a system represented by

$$x_i' = f_i(x_1, \ldots, x_n, u), \qquad i = 1 \text{ to } n,$$

where $x_1, \ldots, x_n$ are the system's state variables and $u = (u_1, \ldots, u_m)$ is the control vector. The optimization criterion is $J = x_0(t_f)$, where

$$x_0(t) = \int_0^t f_0(x, u)dt,$$

and $x = (x_0, x_1, \ldots, x_n)$. Further, the *costate* vector $\psi = (\psi_0, \ldots, \psi_n)$ is defined by $\psi' = -\partial f/\partial x^T \psi$, and $\psi_0 = -1$, arbitrarily. A *Hamiltonian* is defined $H(\psi, x, u) = \psi^T f(x, u)$. Then a necessary condition for the optimality of u is that it maximizes $H(\psi, x, u)$. For the case of continuous action without saturation (of u), we consider the us that satisfy $\partial H(\psi, x, u)/\partial u_i = 0$ (for all i). For the preshape model, the system's state is described by the separation of the thumb and index finger during the pinch grip. As discussed in Section 3.2, the optimization criterion is based on a weighted sum of the aperture (x_1) and its acceleration (u). Thus we have

$$x_0(t) = \int_0^t (x_1^2 + w\,u^2)dt;$$

and the dynamics of the system are described by

$$\begin{aligned} x_1' &= x_2 \qquad (x_1 \text{ is position}), \\ x_2' &= u \qquad (x_2 \text{ is velocity}). \end{aligned}$$

From the above definition of ψ', we find

$$\begin{aligned} \psi_1' &= 2x_1. \\ \psi_2' &= -\psi_1. \end{aligned}$$

Applying the definition of $H(\psi, x, u)$, we have,

$$H(u) = -(x_1^2 + w\,u^2) + \psi_1 x_2 + \psi_2 u,$$

which we maximize by differentiating with respect to u and equating to zero,

$$0 = -2w\,u + \psi_2,$$

from which

$$2w\,u = \psi_2.$$

This extremum is a maximum, because the second derivative of H is negative, specifically, $\delta^2 H/\delta u^2 = -2w$. We can collect the relevant equations:

$$x_1' = x_2. \tag{A.7a}$$

$$x_2' = u = 1/(2w)\psi_2. \tag{A.7b}$$

$$\psi_2' = -\psi_1. \tag{A.7c}$$

$$\psi_1' = 2x_1. \tag{A.7d}$$

Through substitution, this can be written as the following single, fourth-order differential equation in terms of the driving signal $u(t)$:

$$\tau^4 u'''' + u = 0 \qquad (\tau^4 = w),$$

the solution of which is,

$$u(t) = \frac{1}{\tau^2}[e^r(-a_1 \sin r + a_2 \cos r) + e^{-r}(a_3 \sin r - a_4 \cos r)], \quad \text{(A.8)}$$

where $r = (1/\sqrt{2}\tau)\, t$, and a_1 to a_4 are parameters determined by boundary conditions. To determine these, we write the following four boundary equations:

$$x_1(0) = x_1^\circ \quad \text{(initial finger aperture)}, \qquad \text{(A.9a)}$$

$$x_2(0) = 0 \quad \text{(initial finger aperture velocity)}, \qquad \text{(A.9b)}$$

$$x_1(D) = x_1^f \quad \text{(final finger aperture)}, \qquad \text{(A.9c)}$$

$$x_2(D) = 0 \quad \text{(final finger aperture velocity)}, \qquad \text{(A.9d)}$$

where $D = t_f - t_o$. Integrating (A.8) twice (following Equations A.7a, b), we have

$$x_1(t) = e^r(a_1 \cos r + a_2 \sin r) + e^{-r}(a_3 \cos r + a_4 \sin r). \quad \text{(A.10a)}$$

$$x_2(t) = \frac{1}{\sqrt{2}\tau}\Big\{e^r[(a_2 - a_1)\sin r + (a_1 + a_2)\cos r] + e^{-r}[(a_3 - a_4)\sin r + (-a_3 + a_4)\cos r]\Big\}. \quad \text{(A.10b)}$$

Combining Equations A.9 and A.10,

$$x_1^\circ = a_1 + a_3, \qquad \text{(A.11a)}$$

$$x_2^\circ = \frac{1}{\sqrt{2}\tau}(a_1 + a_2 - a_3 + a_4), \qquad \text{(A.11b)}$$

$$x_1^f = \alpha a_1 1 + \beta a_2 + \gamma a_3 + \delta a_4, \qquad \text{(A.11c)}$$

$$0 = \frac{1}{\sqrt{2}\tau}[\alpha(a_1 + a_2) + \beta(a_2 - a_1) + \gamma(a_4 - a_3) + \delta(-a_3 - a_4)], \quad \text{(A.11d)}$$

where, as a shorthand, we use $\alpha = e^{D'}\cos D'$, $\beta = e^{D'}\sin D'$, $\gamma = e^{-D'}\cos D'$, $\delta = e^{-D'}\sin D'$, and $D' = (1/\sqrt{2}\tau)D$. The parameters a_1–a_4 then come as the solution to the matrix equation,

$$\begin{bmatrix} x_1^f \\ 0 \\ x_1^\circ \\ \sqrt{2}\tau x_2^\circ \end{bmatrix} = \begin{bmatrix} \alpha & \beta & \gamma & \delta \\ \alpha-\beta & \alpha+\beta & -\gamma-\delta & \gamma-\delta \\ 1 & 0 & 1 & 0 \\ 1 & 1 & -1 & 1 \end{bmatrix} \begin{bmatrix} a_1 \\ a_2 \\ a_3 \\ a_4 \end{bmatrix}. \quad \text{(A.12)}$$

Following the controller derivation in Section 2.2, we wish to find the initial value of the driving signal (after which the initial value will be taken as the current time). Thus we turn to Equation A.8, setting $t = 0$,

$$u(0) = (1/\tau^2)(a_2 - a_4).$$

Inserting the values for a_2 and a_4, which come from Equation A.12,

$$u(0) = \frac{-1}{\det \tau^2}[x_1^\circ(e^{2D'} + e^{-2D'} - 2\cos 2D') + \sqrt{2}\tau x_2^\circ(e^{2D'} - e^{-2D'}) + x_1^f 4\sin D'(e^{-D'} - e^{D'})]. \quad \text{(A.13)}$$

where $det = e^{2D'} + e^{-2D'} - 2 - 4\sin^2 D'$. Thus, as in Equation A.2 for transport, we have a mapping from the current (initial) state of the system and the remaining movement duration (D) into the driving function to be emitted by a controller. Equation A.13 describes the operation of the preshape feedback controller of Figure 5.

ACKNOWLEDGMENT

Preparation of this article was supported in part by a grant from the Human Frontier Science Program. We express our warm thanks to Marc Jeannerod and Claude Prablanc for their hospitality, and for their discussion of the results, which stimulated the present modeling.

NOTES

1. This article also reviews various other models of centrally programmed reaching, such as the vector integration to end point (VITE) model (Bullock & Grossberg, 1988) and an iterative correction model (Craik, 1947; Jeannerod, 1988; Meyer, Keith, & Wright, 1982), and reviews differing concepts of motor program (Arbib, 1981; Schmidt, 1982).

2. Note, however, the difference between motor control in free space and when interacting with the environment: In grasping and mug placing (Arbib, Iberall, & Lyons, 1985), there is a distinct contact phase, in which the subject attends to tactile/force feedback. Here we restricted ourselves to the free space paradigm.

3. To emphasize the simplicity of the computation performed, they offered a simple artificial neural network construct, which can be adapted for this purpose.

4. All time values given are relative to movement onset, which was coincident with target perturbation. The time values were intersubject averages.

REFERENCES

Arbib, M. A. (1981). Perceptual structures and distributed motor control. In V. B. Brooks (Ed.), *Handbook of physiology: Sec. 1. The nervous system: Vol. 2. Motor control* (pp. 1449–1480). Bethesda, MD: American Physiological Society.

Arbib, M. A., Iberall, T., & Lyons, D. (1985). Coordinated control programs for control of the hands. In A. W. Goodwin & I. Darian-Smith (Eds.), *Hand function and the neocortex. Experimental Brain Research (Suppl) 10* (pp. 111–129).

Atkeson, C. G., & Hollerbach, J. M. (1985). Kinematic features of unrestrained vertical arm movements. *Journal of Neuroscience, 5*, 2318–2330.

Bullock, D., & Grossberg, S. (1988). Neural dynamics of planned arm movements: Emergent invariants and speed-accuracy properties during trajectory formation. In S. Grossberg (Ed.), *Neural networks and natural intelligence* (pp. 553–622). Cambridge, MA: MIT Press.

Craik, K. J. W. (1947). Theory of the human operator in control systems. I. The operator as an engineering system. *British Journal of Psychology, 38*, 56–61.

Crossman, E. R. F. W., & Goodeve, P. J. (1983). Feedback control of hand-movement and Fitts' law. *Quarterly Journal of Experimental Psychology, 35A*, 251–278.

Flash, T. (1987). The control of hand equilibrium trajectories in multi-joint arm movements. *Biological Cybernetics, 57*, 257–274.

Flash, T., & Henis, E. (1992). Arm trajectory modification during reaching towards visual targets. *Journal of Cognitive Neuroscience, 3*, 220–230.

Flash, T., & Hogan, N. (1985). The coordination of arm movements: An experimentally confirmed and mathematical model. *Journal of Neuroscience, 5*, 1688–1703.

Fuchs, A. F., & Kaneko, C. R. S., & Scudder, C. A. (1985). Brainstem control of saccadic eye movements, *Annual Review of Neuroscience, 8*, 307–337.

Gentilucci, M., Chieffi, S., Scarpa, M., & Castiello, U. (1992). Temporal coupling between transport and grasp components during prehension movements: Effects of visual perturbation. *Behavioral Brain Research, 47*, 71–82.

Georgopoulos, A. P., Kalaska, J. F., & Massey, J. T. (1981). Spatial trajectories and reaction times of aimed movements: Effects of practice, uncertainty, and change in target location. *Journal of Neurophysiology, 46*, 725–743.

Hoff, B. (1992). *A computational description of the organization of human reaching and prehension* (Tech. Rep. No. USC-CS-92-523, USC-CNE-92-02). Los Angeles, University of Southern California.

Hoff, B., & Arbib, M. A. (1991). A model of the effects of speed, accuracy and perturbation on visually guided reaching. In R. Caminiti (Ed.), *Control of arm movement in space: Neurophysiological and computational approaches*, Experimental Brain Research Series. New York: Springer-Verlag.

Hogan, N. (1984). An organizing principle for a class of voluntary movements. *Journal of Neuroscience, 4*, 2745–2754.

Jeannerod, M. (1981). Intersegmental coordination during reaching at natural visual objects. In J. Long & A. Baddeley, (Eds.), *Attention and performance IX* (pp. 153–168). Hillsdale, NJ: Erlbaum.

Jeannerod, M. (1984). The timing of natural prehension movements. *Journal of Motor Behavior, 16*, 235–254.

Jeannerod, M. (1988). *The neural and behavioral organization of goal-directed movements*. Oxford: Clarendon.

Jeannerod, M., & Biguer, B. (1982). Visuomotor mechanisms in reaching within extrapersonal space. In D. J. Ingle, R. J. W. Mansfield, & M. A. Goodale, (Eds.), *Advances in the analysis of visual behavior* (pp. 387–409). Cambridge, MA: MIT Press.

Kawato, M., Miyamoto, H., Setoyama, T., & Suzuki, R. (1988). Feedback-error-learning neural network for trajectory control of a robotic manipulator. *Neural Networks, 1*, 256–265.

MacKenzie, C. L., Marteniuk, R. G., Dugas, C., Liske, D., & Eickmeier, B. (1987). Three-dimensional movement trajectories in Fitts' task: Implications for control. *Quarterly Journal of Experimental Psychology, 39A*, 629–647.

Marteniuk, R. G., Leavitt, J. L., MacKenzie, C. L., & Athenes, S. (1990). Functional relationships between grasp and transport components in a prehension task. *Human Movement Science, 9*, 149–176.

Meyer, D. E., Abrams, R. A., Kornblum, S., Wright, C. E., & Smith, J. E. K. (1988). Optimality in human motor performance: Ideal control of rapid aimed movements. *Psychological Reviews, 95*, 340–370.

Meyer, D. E., Keith, J. E. K., & Wright, C. E. (1982). Models for the speed and accuracy of aimed movements. *Psychological Reviews, 89*, 449–482.

Milner, T. E., & Ijaz, M. M. (1990). The effect of accuracy constraints on three-dimensional movement kinematics. *Neuroscience, 35*, 365–374.

Paulignan, Y., Jeannerod, M., MacKenzie, C., & Marteniuk, R. (1991). Selective perturbation of visual input during prehension movements. 2. The effects of changing object size. *Experimental Brain Research, 87*, 407–420.

Paulignan, Y., MacKenzie, C., Marteniuk, R., & Jeannerod, M. (1991). Selective perturbation of visual input during prehension movements. 1. The effects of changing object position. *Experimental Brain Research, 83*, 502–512.

Pélisson, D., Prablanc, C., Goodale, M. A., & Jeannerod, M. (1986). Visual control of reaching movements without vision of the limb: II. Evidence of fast, unconscious processes correcting the trajectory of the hand to the final position of a double-step stimulus. *Experimental Brain Research, 62*, 303–311.

Rogal, L., & Fischer, B. (1986). Eye-hand coordination: A model for computing reaction times in a visually guided reach task. *Biological Cybernetics, 55*, 263–273.

Schmidt, R. A. (1982). The schema concept. In J. A. S. Kelso (Ed.), *Human motor behavior, an introduction* (pp. 219–235). Hillsdale, NJ: Erlbaum.

Schmidt, R. A., Zelaznik, H. N., & Frank, J. S. (1977). Motor output variability: An alternative interpretation of Fitts' law. *Big 10 Symposium on Information Processing in Motor Learning and Control*, University of Wisconsin-Madison, 15 April 1978.

Takahashi, Y., Rabins, M. J., & Auslander, D. M. (1970). *Control and dynamic systems*. Reading, MA: Addison-Wesley.

Uno, Y., Kawato, M., & Suzuki, R. (1989). Formation and control of optimal trajectory in human multijoint arm movement—A minimum torque-change model. *Biological Cybernetics, 61*, 89–101.

Van der Houwen, P. J. (1977). *Construction of integration formulas for initial value problems*. Amsterdam: North-Holland.

Wing, A. M., Turton, A., & Fraser, C. (1986). Grasp size and accuracy of approach in reaching. *Journal of Motor Behavior, 18*, 245–260.

Woodworth, R. S. (1899). The accuracy of voluntary movements. *Psychological Reviews Monograph Supplement, 3*, 1–114.

Submitted December 26, 1991
Revised September 22, 1992